



Published in final edited form as:

Diabetologia. 2023 March ; 66(3): 567–578. doi:10.1007/s00125-022-05838-8.

Distinct subcellular localisation of intramyocellular lipids and reduced PKC ϵ /PKC θ activity preserve muscle insulin sensitivity in exercise-trained mice

Rafael C. Gaspar^{1,2}, Kun Lyu^{1,3}, Brandon T. Hubbard^{1,3}, Brooks P. Leitner^{1,3}, Panu K. Luukkonen¹, Sandro M. Hirabara^{1,4}, Ikki Sakuma¹, Ali Nasiri¹, Dongyan Zhang¹, Mario Kahn¹, Gary W. Cline¹, José Rodrigo Pauli², Rachel J. Perry^{1,3}, Kitt F. Petersen¹, Gerald I. Shulman^{1,3}

¹Department of Internal Medicine, Yale School of Medicine, New Haven, CT, USA

²School of Applied Science, University of Campinas, Limeira, SP, Brazil

³Department of Cellular & Molecular Physiology, Yale School of Medicine, New Haven, CT, USA

⁴Institute of Physical Activity Science and Sports, Cruzeiro do Sul University, São Paulo, SP, Brazil

Abstract

Aims/hypothesis—Athletes exhibit increased muscle insulin sensitivity, despite increased intramuscular triacylglycerol content. This phenomenon has been coined the ‘athlete’s paradox’ and is poorly understood. Recent findings suggest that the subcellular distribution of *sn*-1,2-diacylglycerols (DAGs) in the plasma membrane leading to activation of novel protein kinase Cs (PKCs) is a crucial pathway to inducing insulin resistance. Here, we hypothesised that regular aerobic exercise would preserve muscle insulin sensitivity by preventing increases in plasma membrane *sn*-1,2-DAGs and activation of PKC ϵ and PKC θ despite promoting increases in muscle triacylglycerol content.

Methods—C57BL/6J mice were allocated to three groups (regular chow feeding [RC]; high-fat diet feeding [HFD]; RC feeding and running wheel exercise [RC-EXE]). We used a novel LC-MS/MS/cellular fractionation method to assess DAG stereoisomers in five subcellular compartments (plasma membrane [PM], endoplasmic reticulum, mitochondria, lipid droplets and cytosol) in the skeletal muscle.

Results—We found that the HFD group had a greater content of *sn*-DAGs and ceramides in multiple subcellular compartments compared with the RC mice, which was associated with an increase in PKC ϵ and PKC θ translocation. However, the RC-EXE mice showed, of

✉ Gerald I. Shulman, gerald.shulman@yale.edu.

Contribution statement All the authors contributed substantially to the conception and design; data acquisition or analysis; interpretation of data; and drafting of the article or revising it critically for important intellectual content. All authors approved the final version to be published. RCG and GIS are guarantors of this study and accept full responsibility for the conduct of the study.

Authors’ relationships and activities The authors declare that there are no relationships or activities that might bias, or be perceived to bias, their work.

Supplementary Information The online version contains peer-reviewed but unedited supplementary material available at <https://doi.org/10.1007/s00125-022-05838-8>.

particular note, a reduction in PM *sn*-1,2-DAG and ceramide content when compared with HFD mice. Consistent with the PM *sn*-1,2-DAG–novel PKC hypothesis, we observed an increase in phosphorylation of threonine¹¹⁵⁰ on the insulin receptor kinase (IRK^{T1150}), and reductions in insulin-stimulated IRK^{Y1162} phosphorylation and IRS-1-associated phosphoinositide 3-kinase activity in HFD compared with RC and RC-EXE mice, which are sites of PKC ϵ and PKC θ action, respectively.

Conclusions/interpretation—These results demonstrate that lower PKC θ /PKC ϵ activity and *sn*-1,2-DAG content, especially in the PM compartment, can explain the preserved muscle insulin sensitivity in RC-EXE mice.

Keywords

Athlete's paradox; Insulin resistance; Physical exercise; PKC ϵ ; PKC θ ; Skeletal muscle

Introduction

Insulin resistance in skeletal muscle plays a critical role in the pathogenesis of type 2 diabetes and cardiometabolic disease and is strongly correlated with increased intramyocellular lipid (IMCL) content in sedentary individuals, which has been postulated to play a major role in causing insulin resistance [1–6]. However, contrary to these findings, athletes have been shown to maintain high skeletal muscle insulin sensitivity despite having similarly high levels of IMCL content [7, 8], a phenomenon coined the ‘athlete’s paradox’.

Novel isoforms of protein kinase C (nPKC) have been suggested as important players in lipid-induced insulin resistance [9–12]. In skeletal muscle, our group and others have shown that novel protein kinase C (PKC) isoforms PKC θ and PKC ϵ are associated with lipid-induced insulin resistance in humans and rodents [8, 13–17]. In recent studies, we found that increases in plasma membrane (PM) *sn*-1,2-diacylglycerol (DAG) were responsible for mediating lipid-induced insulin resistance in the liver, skeletal muscle and white adipose tissue (WAT) through activation of PKC ϵ in all of these tissues as well as PKC θ in skeletal muscle, which in contrast to the other tissues is abundant in skeletal muscle [14, 18, 19]. We went on to demonstrate that PM *sn*-1,2-DAG-induced PKC ϵ activation promotes insulin resistance in these tissues through phosphorylation of threonine¹¹⁵⁰ on the insulin receptor kinase (IRK; that is, IRK^{T1150}), which in turn leads to inhibition of IRK activity, whereas PM *sn*-1,2-DAG-induced PKC θ activation further contributes to insulin resistance in skeletal muscle by causing reductions in insulin-stimulated IRS-1-associated phosphoinositide 3-kinase (PI3-kinase) activity [15].

We therefore hypothesised that the paradoxical effects of physical exercise on muscle triacylglycerol (TAG) content and muscle insulin sensitivity could be explained by differences in PM *sn*-1,2-DAG content, and PKC ϵ /PKC θ activation in the skeletal muscle. To address this hypothesis, we applied a novel LC-MS/MS method to assess the different stereoisomers of DAGs and ceramides in five intracellular compartments along with PKC ϵ /PKC θ activity and insulin signalling/insulin action.

Methods

Animals

All animal studies were approved by the Yale University Institutional Animal Care and Use Committee and were performed in accordance. Male C57BL6 mice (10–12 weeks) acquired from The Jackson Laboratory (USA) were housed in the Yale Animal Resources Center in individual cages at 23°C under 12 h light (7:00 hours to 19:00 hours)/12 h dark cycles (19:00 hours to 7:00 hours). The mice were fed ad libitum with free access to water. To address the hypothesis, we studied three groups: (1) regular chow feeding (RC); (2) high-fat diet feeding (HFD); (3) RC feeding and running wheel (Columbus Instruments, USA) voluntary exercise (RC-EXE). The experimental period was 6 weeks.

OGTTs

After 6 h of fasting, a single dose of 1 g/kg dextrose was administered via gavage, and blood samples were collected from the tail vein at 0, 15, 30, 45, 60 and 120 min to measure plasma glucose and insulin levels.

Plasma and tissue biochemical measurement

Plasma glucose was measured by YSI Glucose Analyzer (Xylem, USA). Plasma insulin was measured by the Yale Diabetes Research Center Radioimmunoassay Core using radioimmunoassay. Plasma NEFA was measured using the enzymatic colorimetric method by Wako reagents (FUJIFILM; Wako Diagnostics, USA). TAG was measured by Sekisui's Triglyceride-SL Reagent (Sekisui Diagnostics, USA). Skeletal muscle and liver TAGs were extracted with cold 2:1 chloroform:methanol (vol./vol.). Samples were then mixed with sulfuric acid (1 mol/l) and centrifuged to achieve phase separation. The organic phase was measured by Sekisui's Triglyceride-SL Reagent.

Mouse hyperinsulinaemic–euglycaemic clamp

The surgery for the hyperinsulinaemic–euglycaemic clamp was performed under isoflurane anaesthesia (5% for induction and 2.5% for maintenance). Jugular venous catheters were placed 6–7 days before the studies. Only mice that recovered to >90% of their pre-operative weight were studied. After 6 h of fasting, awake mice under tail restraint received a 120 min infusion of [$3\text{-}^3\text{H}$]glucose (1.800 Bq/min) to measure basal glucose turnover. The blood sample was collected by tail bleeding at the end of basal infusion to determine plasma glucose, insulin, NEFAs and ^3H -glucose specific activity. Following basal infusion, a 140 min hyperinsulinaemic–euglycaemic clamp was performed with a continuous infusion of insulin at the dose of $2.5\text{ (mU kg}^{-1}\text{ min}^{-1})$ to raise plasma insulin concentrations to simulate postprandial insulin levels. Dextrose (20%) was infused at variable rates to maintain euglycaemia (plasma glucose 5.6–6.7 mmol/l). The dextrose was enriched with [$3\text{-}^3\text{H}$]glucose to measure insulin-stimulated glucose turnover. A bolus (370.000 Bq) of 2-[$1\text{-}^{14}\text{C}$]deoxyglucose (2-DOG) was injected at 85 min to determine the rate of muscle-specific glucose uptake under insulin stimulation. During the clamp, blood samples were collected at 10–25 min intervals for immediate determination of plasma glucose levels. After 2-DOG injection, extra plasma was collected for measuring plasma ^{14}C -glucose specific

activity. At the end of the clamp, plasma was collected to measure plasma glucose, insulin, NEFAs and $^3\text{H}/^{14}\text{C}$ -glucose specific activity [20, 21].

DAG subcellular fractionation

The subcellular fractionation protocol has been previously described [18, 19]. Briefly, gastrocnemius tissues (~100 mg) were homogenised in cold (4°C) TES buffer (250 mmol/l sucrose, 10 mmol/l Tris-pH 7.4, 0.5 mmol/l EDTA) with a Dounce homogeniser. The homogenate was centrifuged (at 17,000 *g*, SS-34 rotor, 15 min, 4°C) to separate pellet A and supernatant A.

Pellet A was resuspended in TES buffer and centrifuged (at 17,000 *g* with SS-34 rotor, 20 min, 4°C). After that, pellet A was resuspended in TES buffer and layered on top of a 1.12 mol/l sucrose buffer. The samples were centrifuged (at 105,000 *g* with TLS-55 rotor, 20 min, 4°C) to separate pellet B, interface B and supernatant B. Pellet B was collected as the mitochondrial fraction. Interface B was collected and resuspended in TES buffer and centrifuged (at 60,000 *g* with TLA100.2 rotor, 9 min, 4°C) to obtain pellet C. Pellet C was resuspended in TES buffer and centrifuged (at 60,000 *g* with TLA100.2 rotor, 9 min, 4°C) and was used as the PM fraction.

Supernatant A was centrifuged (at 390,000 *g* with Ti-70.1 rotor, 75 min, 4°C) to separate pellet D and supernatant D. The top lipid layer was collected as the lipid droplet (LD) fraction. Supernatant D was collected as the cytosol fraction, while pellet D was collected as the endoplasmic reticulum (ER) fraction. Figure 1 shows the separation of the five subcellular compartments in gastrocnemius.

DAGs were extracted from the five fractions and measured by LC-MS/MS as described previously [18, 19].

Western blotting

Gastrocnemius lysates were prepared in RIPA buffer with protease inhibitors (cOmplete MINI; Roche, Switzerland) and phosphatase inhibitors (PhosSTOP; Roche, Switzerland). Protein concentration was determined by the Bradford method (Bradford Reagent; Thermo Scientific, USA). Protein was loaded and resolved by SDS-PAGE using 4–12% gradient gels (Life Technologies, USA) and proteins were transferred to PVDF membranes (MilliporeSigma, USA) by semidry transfer. Membranes were blocked in 5% BSA for 1 h at room temperature and probed overnight at 4°C with primary antibodies (1:1000). The antibody list can be found in detail in the electronic supplementary material (ESM). Films were developed within the linear dynamic range of signal intensity and then were scanned for digital analysis.

IRS-1-associated PI3-kinase activity

IRS-1-associated PI3-kinase activities were measured in gastrocnemius samples after immunoprecipitation with IRS-1 antibody (BD Biosciences, USA). The incorporation of ^{32}P into phosphatidylinositol to yield phosphatidylinositol-3-monophosphate was measured to determine the IRS-1-associated PI3-kinase activity, as previously described [22].

PKC, CD36 and lipoprotein lipase translocation

Gastrocnemius samples were homogenised in buffer A (20 mmol/l Tris-HCl, pH 7.4, 1 mmol/l EDTA, 0.25 mmol/l EGTA, 250 mmol/l sucrose, and protease and phosphatase inhibitors). The lysate was centrifuged (60 min, 100,000g, 4°C), and the supernatant was collected as the cytosolic fraction. The pellet was resuspended in buffer B (250 mmol/l Tris-HCl, pH 7.4, 1 mmol/l EDTA, 0.25 mmol/l EGTA, 2% Triton X-100, and added protease and phosphatase inhibitors) by sonication, and incubated at 4°C for 45 min to solubilise membrane proteins. Next, samples were centrifuged (60 min, 100,000g, 4°C), and the supernatant was saved as the membrane fraction. The protein samples were subjected to western blot analysis as described above. The ratio of membrane fraction to cytosolic fraction was calculated as an index of protein translocation.

Glycogen measurements

To assess the glycogen content, gastrocnemius samples were homogenised in 0.6 mol/l perchloric acid. Part of the homogenate was saved to measure as free glucose. Another part of the homogenate was neutralised by 1 mol/l KHCO₃ and digested with amyloglucosidase (2 mg/ml) dissolved in acetate buffer (0.4 mol/l, pH 4.8) for 2 h at 37–40°C. Glucose levels were analysed in free glucose samples and after the amyloglucosidase digestion (total glucose) to calculate total glycogen content [19].

Statistics

Data are presented as the mean ± SEM. Data normality was analysed by the Shapiro–Wilk W test. For the data with normal distribution, one-way ANOVA followed by Tukey’s post hoc test was used. Kruskal–Wallis nonparametric test was used for non-normal data. Two-way ANOVA and the Tukey post hoc test were adopted to compare all groups in pairs for the OGTT analyses. Differences were considered significant if $p < 0.05$. * $p < 0.05$, ** $p < 0.01$, *** $p < 0.001$ vs RC mice and † $p < 0.05$, †† $p < 0.01$, ††† $p < 0.001$ vs HFD mice. GraphPad Prism 9.4.1 (<https://www.graphpad.com/scientific-software/prism/>, GraphPad Software, USA) was used for the construction of the graphs and for statistical analysis.

Results

Baseline characteristics of mice

We first evaluated the body composition of mice after 6 weeks of HFD, RC or RC-EXE [20]. As designed, the final body weight was higher in HFD mice compared with RC and RC-EXE mice (Table 1). HFD mice had significantly increased fat mass and a reduction in lean body mass compared with the other two groups (Table 1). No difference was observed in the muscle glycogen content among the three groups at baseline (Table 1).

Exercised mice have normal glucose tolerance despite similar muscle TAG content

The weekly and cumulative running distances were calculated from the running wheels during the 6 weeks of running wheel exercise for the RC-EXE mice and demonstrated that the RC-EXE mice ran voluntarily a mean of ~43 km per week and a total distance of ~260 km over 6 weeks prior to the study (Fig. 2a). Consistent with this voluntary exercise, RC-

EXE mice had a slightly increased $\dot{V}O_{2\max}$ rate ($\dot{V}O_{2\text{peak}}$) ($p=0.08$) as well as having a higher speed and time of exhaustion on a graded treadmill test when compared with HFD and RC mice (ESM Fig. 1). We next assessed in direct calorimetry in our experimental model [20]. Under basal conditions, RC and RC-EXE mice exhibited slightly increased rates of $\dot{V}O_2$ and energy expenditure than the HFD mice in the dark cycle (ESM Fig. 2). Compared with HFD mice, carbon dioxide production and the respiratory exchange ratio were higher in the RC and RC-EXE mice without prominent differences in the activity counts (ESM Fig. 2). In addition, HFD mice showed significantly increased concentrations of TAGs in the gastrocnemius and quadriceps muscles compared with RC mice but not when compared with RC-EXE (Fig. 2b, ESM Fig. 1). Conversely, RC-EXE mice demonstrated lower NEFA and TAG levels in the liver when compared with both RC and HFD mice (ESM Fig. 1). Lastly, to better understand the effects of IMCL on glucose metabolism in our model, we performed OGTTs in the three groups of mice. Despite no significant differences in muscle TAG between HFD and RC-EXE mice, the RC-EXE mice manifested normal glucose tolerance and normal plasma insulin concentrations during an OGTT, while the HFD mice showed impaired glucose tolerance and markedly higher plasma insulin concentrations (Fig. 2c,d).

Exercised mice manifest normal insulin sensitivity in muscle despite no significant differences in muscle TAG content compared with HFD mice

We next evaluated whole-body and skeletal muscle insulin sensitivity in these mice. Consistent with the OGTT results the HFD mice exhibited whole-body insulin resistance during the hyperinsulinaemic–euglycaemic clamp, as reflected by a lower glucose infusion rate (GIR) required to maintain euglycaemia during the clamp, while the RC-EXE mice showed normal insulin sensitivity compared with the RC mice (Fig. 3a,b,c). Glucose disposal rate (R_d) in the RC-EXE mice was comparable to the RC mice while being lower in the HFD mice than in RC-EXE (Fig. 3d). Skeletal muscle insulin-stimulated glucose uptake was higher in the RC-EXE mice compared with the HFD mice (Fig. 3e). In addition, no difference was observed in the endogenous glucose production (EGP); however, RC-EXE mice showed a greater suppression of plasma NEFA levels ($p=0.08$) by insulin during the hyperinsulinaemic–euglycaemic clamp compared with the HFD mice (Fig. 3f,g).

Exercised mice have lower PKC ϵ /PKC θ activation and IRK^{T1150} phosphorylation in skeletal muscle compared with HFD mice

Previous studies have demonstrated that lipid-induced skeletal muscle insulin resistance is mediated by PKC ϵ /PKC θ activation in humans and rodents [1, 9]. Consistent with these studies, HFD mice had higher activation compared with the RC mice, while the RC-EXE mice exhibited reduced PKC θ and PKC ϵ activation compared with the HFD mice (Fig. 4a). No changes were found in PKC α , PKC β and PKC δ translocation (ESM Fig. 3). PKC ϵ has been shown to phosphorylate IRK at IRK^{T1150} in rodents (IRK^{T1160} in humans) which in turn leads to reduced IRK activity [14, 18, 19]. Consistent with this model, IRK^{T1150} phosphorylation was also higher in the HFD mice compared with the RC group, while the RC-EXE mice maintained a low level of IRK^{T1150} phosphorylation in the skeletal muscle (Fig. 4b). Furthermore RC-EXE mice manifested increased insulin-stimulated IRK^{Y1162} phosphorylation and IRS-1-associated PI3-kinase activity when compared with the HFD

mice (Fig. 4c,e). Next, we measured insulin-stimulated Akt phosphorylation, which was reduced in HFD mice compared with RC mice (Fig. 4d). We also assessed Akt translocation and p-PKC ζ^{T410} in our experimental model. However, no differences among the groups were observed in Akt translocation or PKC ζ^{T410} phosphorylation (ESM Fig. 3).

***sn*-DAG and ceramide compartmentation is different in exercised mice compared with HFD mice**

Increased concentrations of PM *sn*-1,2-DAGs have been demonstrated to be the key mediators of lipid-induced insulin resistance in several tissues through activation of nPKCs [9, 14, 19]. Consistent with these prior observations, we found that HFD mice had ~twofold higher levels of *sn*-1,2-DAGs in the PM of skeletal muscle compared with the RC mice (Fig. 5a). We also found higher levels of *sn*-1,2-DAGs in the LD, mitochondria (Mito) and cytosol of skeletal muscle in HFD mice compared with the RC mice (Fig. 5a). On the other hand, the RC-EXE mice maintained lower levels of *sn*-1,2 DAGs in the PM but no differences were observed in the other cellular compartments compared with the HFD mice (Fig. 5a). Strikingly, compared with RC mice, HFD mice showed similar increases in the other two DAG stereoisomers (Fig. 5b,c). Conversely, RC-EXE mice manifested lower levels of *sn*-1,3-DAGs in the PM and Mito compartments when compared with HFD mice (Fig. 5b,c). We also assessed ceramides in the same five compartments. Compared with RC, the HFD mice manifested increased ceramide content in the PM, LD and cytosol compartments (Fig. 5d). However, the RC-EXE mice had lower ceramide levels in the PM and ER when compared with HFD mice (Fig. 5d). Finally, we analysed the content of different species of ceramides and observed higher C16:0, C18:0 and C22:0 ceramides in the PM of HFD mice (ESM Fig. 4). HFD mice also had greater C18:0 levels in the LD and cytosol compartments compared with RC mice (ESM Fig. 4). In contrast, the RC-EXE mice demonstrated reductions in C16:0, C18:0, C20:0 and C22:0 ceramides in the PM as well as a lower C18:0 ceramide in the ER and Mito when compared with HFD mice (ESM Fig. 4). Since *sn*-DAG content and PKC ϵ activation can be altered by changes in the fed (insulin-stimulated state) and fasted states [23], we used different sets of mice for each study. Thus, it was not possible to determine the correlation between nPKC activation and insulin signalling.

Exercised mice increased DGAT1 and CD36 in skeletal muscle

To examine the potential mechanism responsible for increased TAG accumulation in the skeletal muscle of RC-EXE mice and HFD mice, we evaluated several key enzymes responsible for fatty acid uptake and TAG synthesis. Expression of diacylglycerol acyltransferase-1 (DGAT1) was higher in the RC-EXE mice compared with the other groups, whereas expression of diacylglycerol acyltransferase-2 (DGAT2) was higher in the HFD mice compared with the other two groups (Fig. 6a). RC-EXE mice showed a higher CD36 protein content compared with both RC and HFD mice (Fig. 6a). We did not observe any differences in lipoprotein lipase (LPL) expression and translocation in these mice (Fig. 6b, ESM Fig. 5). On the other hand, HFD mice showed lower CD36 translocation compared with the RC mice, while the CD36 translocation was higher in exercised mice than in HFD mice (Fig. 6c). In contrast, we did not observe any differences in adipose triglyceride

lipase (ATGL) or hormone-sensitive lipase (HSL) phosphorylation (ESM Fig. 5) among the groups.

Discussion

Increased IMCL content is strongly associated with muscle insulin resistance in sedentary individuals and is likely a biomarker for related lipid metabolites (e.g. DAGs, ceramides, etc.) that mediate insulin resistance [5]. However, an important exception to this relationship occurs in athletes who typically manifest increased IMCL content despite maintaining normal or increased muscle insulin sensitivity, a phenomenon coined the athlete's paradox [24–26]. In this regard, recent studies have demonstrated that specific increases in *sn*-1,2-DAGs in the PM lead to increased nPKC activation and insulin resistance in the liver, WAT and skeletal muscle [14, 18, 19] independent of changes in TAG content.

To test this hypothesis in our model, we measured the translocation of PKCs/nPKCs, and the activation of key steps of the insulin signalling pathway as well as PM *sn*-1,2-DAG content, key activators of nPKC translocation [27, 28]. Here we show that despite similar TAG levels in skeletal muscle of HFD and RC-EXE mice, RC-EXE mice manifested lower levels of especially PM *sn*-1,2-DAG content, which was associated with reduced PKC ϵ and PKC θ translocation compared with the HFD mice. Strikingly, HFD mice showed increases in *sn*-DAG isoforms and ceramides in multiple subcellular compartments which were not observed in the RC-EXE group. Further, we observed that this protection from lipid-induced muscle insulin resistance in the RC-EXE mice was associated with a reduction in IRK^{T1150} phosphorylation and increases in insulin-stimulated IRK^{Y1162} phosphorylation consistent with the *sn*-1,2-DAG–PKC ϵ –IRK^{T1150} phosphorylation pathway of lipid-induced insulin resistance [14, 18, 19].

In contrast to our findings, Perreault et al did not observe an association between sarcolemma *sn*-1,2-DAG content and insulin resistance [8]. These different results may be due to technical differences in the methods used to isolate skeletal muscle in the two studies. The muscle biopsy procedure used by Perreault et al (2018), which included extramuscular fat dissection, might result in some degree of warm ischaemia and breakdown of *sn*-DAGs. In our study, we performed in situ freeze-clamping of skeletal muscle with aluminium tongs precooled in liquid nitrogen to minimise DAG hydrolysis due to warm ischaemia. Furthermore, in contrast to the study by Perreault et al, we also assessed the effects of exercise and high-fat feeding on insulin signalling IRK^{Y1162} phosphorylation and IRS-1-associated PI3-kinase. In addition we also assessed IRK^{T1150} phosphorylation, a direct target of PKC ϵ and PKC θ translocation, which has been shown to mediate *sn*-1,2-DAG-induced muscle insulin resistance at the level of IRS-1-associated PI3-kinase [14, 22].

Alterations in muscle lipid storage have also been observed in individuals with type 2 diabetes, who were found to store lipids in the subsarcolemmal, in larger LDs, especially in type II fibres [7]. On the other hand, athletes predominately store lipids in type I fibres, in the intramyofibrillar region, but a higher number of LDs [7]. Most recently, Sarabhai et al (2022) showed that a single meal containing safflower oil and palm oil induced whole-body and hepatic insulin resistance in healthy volunteers [29]. In the skeletal muscle,

the lipid meal led to an increase in DAG species in the membrane as well as in the LD compartment [29]. Interestingly, PKC θ translocation was increased in both the safflower and palm oil groups, whereas PKC ϵ translocation increased in the palm oil-fed group and tended to increase in the safflower group [29]. The palm oil group also showed an increase in ceramides associated with greater PKC ζ translocation and phosphatase 2A (PP2A) expression [29].

We also observed that the ceramide species C16:0 and C18:0 were higher in the HFD mice compared with the RC-EXE mice. Ceramide inhibitory action on insulin signalling is thought to occur further downstream of insulin signalling at the level of Akt phosphorylation, which may occur particularly through impairments in Akt translocation, dephosphorylation of Akt by protein PP2A or by PKC ζ phosphorylation [19, 30, 31]. In our study, we did not observe any difference in Akt translocation and PKC ζ phosphorylation among the groups, whereas the HFD mice showed lower p-Akt^{S473} compared with RC mice. The alterations in ceramide content could also have contributed to the observed changes in insulin resistance in these mice, but cannot explain the observed changes in insulin-stimulated IRK^{Y1162} phosphorylation, IRS-1-associated PI3-kinase activity or IRK^{T1150} phosphorylation.

In addition to translocation/activation of the nPKC isoforms, we also assessed translocation of the classical PKC isoforms in this study. We did not observe any differences in the classical PKC isoforms among the groups. In contrast with our findings, Jani and collaborators [30] evaluated PKC δ translocation in the soleus, extensor digitorum longus (EDL) and epitrochlearis muscles after 8 weeks of HFD. They observed that PKC δ translocation was increased in the soleus and EDL muscles, which was associated with increased accumulation of both DAG and ceramide content in those tissues [30]. Since the *sn*-1,3-DAGs are mostly derived from TAG lipolysis and are not able to activate nPKCs [31], our results suggested that the PM *sn*-1,2-DAGs are responsible for mediating the differences in insulin sensitivity in our models through the activation of nPKCs, as previously described [27, 28].

In order to understand potential mechanisms by which HFD and exercise might lead to differences in DAG and ceramide cellular compartmentation, we also analysed expression of DGAT1 and DGAT2, which are critical enzymes in the re-esterification pathway. We found that RC-EXE mice showed increases in DGAT1 protein content when compared with RC and HFD mice. On the other hand, compared with the other groups, HFD mice showed increased DGAT2 protein levels. A previous study reported that exercised mice had increased muscle diacylglycerol acyltransferase (DGAT) activity and that overexpression of DGAT1 in skeletal muscle increased the muscle TAG and protected mice from HFD-induced insulin resistance, reproducing the athlete's paradox phenomenon [32]. Six weeks of running wheel access was also able to increase TAG levels in the skeletal muscle of female mice [33]. In contrast, overexpression of DGAT2 in skeletal muscle was associated with increased lipid content and consequently glucose intolerance [34]. Further, in agreement with our studies, a single bout of or chronic physical exercise can induce increases in CD36 expression in skeletal muscle [35–37]. Interestingly, CD36 knockout mice have attenuated aerobic exercise capacity, which indicates that CD36 is a crucial molecule for

maintaining endurance running capacity [38–40]. Taken together, these data suggest that increased expression of CD36 in RC-EXE mice may contribute to increased muscle fatty acid uptake as reflected by reductions in the plasma NEFA levels. Further, increased DGAT1 expression in RC-EXE mice may promote increased muscle TAG content and reduced PM *sn*-1,2-DAG content in the mice by a pull mechanism.

In summary, our data demonstrate that despite TAG content in skeletal muscle, voluntary exercise in mice resulted in: (1) normal muscle insulin sensitivity in the RC-EXE mice compared with the HFD mice; (2) reductions in PM *sn*-1,2-DAG content and PKC ϵ and PKC θ translocation/activation in skeletal muscle of the RC-EXE mice compared with the HFD mice; (3) reductions in PKC ϵ translocation associated with reduced IRK^{T1150} phosphorylation in the RC-EXE mice compared with the HFD mice; (4) reductions in PKC ϵ and PKC θ translocation/activation in skeletal muscle of RC-EXE mice compared with HFD mice, leading to increased insulin-stimulated IRK^{Y1162} phosphorylation and IRS-1-associated PI3-kinase activity; and (5) lower ceramide content in RC-EXE mice compared with HFD mice, although no differences were observed among the groups for Akt translocation or PKC ζ ^{T410} phosphorylation, which are thought to mediate ceramide-induced insulin resistance. Taken together, these data suggest that lower PM *sn*-1,2-DAG content and lower PKC ϵ /PKC θ activity in skeletal muscle could provide an explanation for the preserved insulin sensitivity in exercised mice despite their intramuscular TAG content.

Supplementary Material

Refer to Web version on PubMed Central for supplementary material.

Acknowledgements

The graphical abstract was drawn by using pictures from Servier Medical Art. Servier Medical Art by Servier is licensed under a Creative Commons Attribution 3.0 Unported License.

Funding

This study was supported by grants from the São Paulo Research Foundation (FAPESP; Process Nos. 2017/20542-3; 2019/11338-9; 2020/13443-1) and the United States Public Health Service (R01 DK116774, R01 DK119968, R01 DK113984, P30 DK045735, T32 GM007205 and R01 DK092661) and a VA Merit award (I01 BX000901).

Data availability

The original data generated during the current study are available from the corresponding author on reasonable request.

Abbreviations

DAG	Diacylglycerol
DGAT1	Diacylglycerol acyltransferase-1
DGAT2	Diacylglycerol acyltransferase-2
2-DOG	2-[1- ¹⁴ C]deoxyglucose

EDL	Extensor digitorum longus
EGP	Endogenous glucose production
ER	Endoplasmic reticulum
GIR	Glucose infusion rate
HFD	High-fat diet feeding
IMCL	Intramyocellular lipid
IRK	Insulin receptor kinase
LD	Lipid droplet
LPL	Lipoprotein lipase
Mito	Mitochondria
nPKC	Novel protein kinase C
PI3-kinase	Phosphoinositide 3-kinase
PKC	Protein kinase C
PM	Plasma membrane
PP2A	Phosphatase 2A
RC	Regular chow feeding
RC-EXE	RC feeding and running wheel voluntary exercise
R_d	Disposal rate
TAG	Triacylglycerol
WAT	White adipose tissue

References

1. Petersen MC, Shulman GI (2018) Mechanisms of insulin action and insulin resistance. *Physiol Rev* 98(4):2133–2223. 10.1152/physrev.00063.2017 [PubMed: 30067154]
2. Laurens C, Moro C (2016) Intramyocellular fat storage in metabolic diseases. *Horm Mol Biol Clin Investig* 26(1):43–52. 10.1515/hmbci-2015-0045
3. Shulman GI (2014) Ectopic fat in insulin resistance, dyslipidemia, and cardiometabolic disease. *N Engl J Med* 371(12):1131–1141. 10.1056/nejmra1011035 [PubMed: 25229917]
4. Weiss R, Dufour S, Taksali SE et al. (2003) Prediabetes in obese youth: a syndrome of impaired glucose tolerance, severe insulin resistance, and altered myocellular and abdominal fat partitioning. *Lancet* 362(9388):951–957. 10.1016/S0140-6736(03)14364-4 [PubMed: 14511928]
5. Krssak M, Falk Petersen K, Dresner A et al. (1999) Intramyocellular lipid concentrations are correlated with insulin sensitivity in humans: a ¹H NMR spectroscopy study. *Diabetologia* 42(1):113–116. 10.1007/s001250051123 [PubMed: 10027589]

6. Dresner A, Laurent D, Marcucci M et al. (1999) Effects of free fatty acids on glucose transport and IRS-1-associated phosphatidylinositol 3-kinase activity. *J Clin Invest* 103(2):253–259. 10.1172/JCI5001 [PubMed: 9916137]
7. Daemen S, Gemmink A, Brouwers B et al. (2018) Distinct lipid droplet characteristics and distribution unmask the apparent contradiction of the athlete's paradox. *Mol Metab* 17:71–81. 10.1016/j.molmet.2018.08.004 [PubMed: 30174227]
8. Perreault L, Newsom SA, Strauss A et al. (2018) Intracellular localization of diacylglycerols and sphingolipids influences insulin sensitivity and mitochondrial function in human skeletal muscle. *JCI Insight* 3(3):e96805. 10.1172/jci.insight.96805 [PubMed: 29415895]
9. Petersen MC, Shulman GI (2017) Roles of diacylglycerols and ceramides in hepatic insulin resistance. *Trends Pharmacol Sci* 38(7):649–665. 10.1016/j.tips.2017.04.004 [PubMed: 28551355]
10. Batista TM, Haider N, Kahn CR (2021) Defining the underlying defect in insulin action in type 2 diabetes. *Diabetologia* 64(5):994–1006. 10.1007/s00125-021-05415-5 [PubMed: 33730188]
11. White MF, Kahn CR (2021) Insulin action at a molecular level – 100 years of progress. *Mol Metab* 52(July):101304. 10.1016/j.molmet.2021.101304 [PubMed: 34274528]
12. Roden M, Shulman GI (2019) The integrative biology of type 2 diabetes. *Nature* 576(7785):51–60. 10.1038/s41586-019-1797-8 [PubMed: 31802013]
13. Szendroedi J, Yoshimura T, Phielix E et al. (2014) Role of diacylglycerol activation of PKC θ in lipid-induced muscle insulin resistance in humans. *Proc Natl Acad Sci* 111(26):9597–9602. 10.1073/pnas.1409229111 [PubMed: 24979806]
14. Song JD, Alves TC, Befroy DE et al. (2020) Dissociation of muscle insulin resistance from alterations in mitochondrial substrate preference. *Cell Metab* 32(5):726–735.e5. 10.1016/j.cmet.2020.09.008 [PubMed: 33035493]
15. Li Y, Soos TJ, Li X et al. (2004) Protein kinase C θ inhibits insulin signaling by phosphorylating IRS1 at Ser1101. *J Biol Chem* 279(44):45304–45307. 10.1074/jbc.C400186200 [PubMed: 15364919]
16. Itani SI, Pories WJ, MacDonald KG, Dohm GL (2001) Increased protein kinase C theta in skeletal muscle of diabetic patients. *Metabolism* 50(5):553–557. 10.1053/meta.2001.22512 [PubMed: 11319716]
17. Griffin ME, Marcucci MJ, Cline GW et al. (1999) Free fatty acid-induced insulin resistance is associated with activation of protein kinase C θ and alterations in the insulin signaling cascade. *Diabetes* 48(6):1270–1274. 10.2337/diabetes.48.6.1270 [PubMed: 10342815]
18. Lyu K, Zhang D, Song J et al. (2021) Short-term overnutrition induces white adipose tissue insulin resistance through sn-1,2-diacylglycerol/PKC ϵ /insulin receptor Thr1160 phosphorylation. *JCI insight* 6(4):e139946. 10.1172/jci.insight.139946 [PubMed: 33411692]
19. Lyu K, Zhang Y, Zhang D et al. (2020) A membrane-bound diacylglycerol species induces PKC ϵ -mediated hepatic insulin resistance. *Cell Metab* 32(4):654–664.e5. 10.1016/j.cmet.2020.08.001 [PubMed: 32882164]
20. Camporez JP, Lyu K, Goldberg EL et al. (2019) Anti-inflammatory effects of oestrogen mediate the sexual dimorphic response to lipid-induced insulin resistance. *J Physiol* 597(15):3885–3903. 10.1113/JP277270 [PubMed: 31206703]
21. Kim JK (2009) Hyperinsulinemic–euglycemic clamp to assess insulin sensitivity in vivo. In: Stocker C (ed) *Type 2 diabetes methods and protocols*. Humana Press, New Jersey, pp 221–238
22. Kim JK, Fillmore JJ, Sunshine MJ et al. (2004) PKC- θ knockout mice are protected from fat-induced insulin resistance. *J Clin Invest* 114(6):823–827. 10.1172/JCI200422230 [PubMed: 15372106]
23. Perry RJ, Wang Y, Cline GW et al. (2018) Leptin mediates a glucose-fatty acid cycle to maintain glucose homeostasis in starvation. *Cell* 172(1–2):234–248.e17. 10.1016/j.cell.2017.12.001 [PubMed: 29307489]
24. Goodpaster BH, He J, Watkins S, Kelley DE (2001) Skeletal muscle lipid content and insulin resistance: evidence for a paradox in endurance-trained athletes. *J Clin Endocrinol Metab* 86(12):5755–5761. 10.1210/jcem.86.12.8075 [PubMed: 11739435]

25. Amati F, Dubé JJ, Alvarez-Carnero E et al. (2011) Skeletal muscle triglycerides, diacylglycerols, and ceramides in insulin resistance. *Diabetes* 60(10):2588–2597. 10.2337/db10-1221 [PubMed: 21873552]
26. Li X, Li Z, Zhao M et al. (2019) Skeletal muscle lipid droplets and the athlete's paradox. *Cells* 8(3):249. 10.3390/cells8030249 [PubMed: 30875966]
27. Boni LT, Rando RR (1985) The nature of protein kinase C activation by physically defined phospholipid vesicles and diacylglycerols. *J Biol Chem* 260(19):10819–10825. 10.1016/S0021-9258(19)85156-6 [PubMed: 3161882]
28. Rando RR, Young N (1984) The stereospecific activation of protein kinase C. *Biochem Biophys Res Commun* 122(2):818–823. 10.1016/S0006-291X(84)80107-2 [PubMed: 6235812]
29. Sarabhai T, Koliaki C, Mastrototaro L et al. (2022) Dietary palmitate and oleate differently modulate insulin sensitivity in human skeletal muscle. *Diabetologia* 65(2):301–314. 10.1007/s00125-021-05596-z [PubMed: 34704121]
30. Jani S, Da Eira D, Hadday I et al. (2021) Distinct mechanisms involving diacylglycerol, ceramides, and inflammation underlie insulin resistance in oxidative and glycolytic muscles from high fat-fed rats. *Sci Rep* 11(1):19160. 10.1038/s41598-021-98819-7 [PubMed: 34580412]
31. Eichmann TO, Kumari M, Haas JT et al. (2012) Studies on the substrate and stereo/regioselectivity of adipose triglyceride lipase, hormone-sensitive lipase, and diacylglycerol-O-acyltransferases. *J Biol Chem* 287(49):41446–41457. 10.1074/jbc.M112.400416 [PubMed: 23066022]
32. Liu L, Zhang Y, Chen N, Shi X, Tsang B, Yu YH (2007) Upregulation of myocellular DGAT1 augments triglyceride synthesis in skeletal muscle and protects against fat-induced insulin resistance. *J Clin Invest* 117(6):1679–1689. 10.1172/JCI30565 [PubMed: 17510710]
33. Morton TL, Galior K, McGrath C et al. (2016) Exercise increases and browns muscle lipid in high-fat diet-fed mice. *Front Endocrinol (Lausanne)* 7:1–8. 10.3389/fendo.2016.00080 [PubMed: 26869991]
34. Levin MC, Monetti M, Watt MJ et al. (2007) Increased lipid accumulation and insulin resistance in transgenic mice expressing DGAT2 in glycolytic (type II) muscle. *Am J Physiol Metab* 293(6):E1772–E1781. 10.1152/ajpendo.00158.2007
35. Łukaszuk B, Bialuk I, Górski J, Zaj czkiewicz M, Winnicka MM, Chabowski A (2012) A single bout of exercise increases the expression of glucose but not fatty acid transporters in skeletal muscle of IL-6 KO mice. *Lipids* 47(8):763–772. 10.1007/s11745-012-3678-x [PubMed: 22623023]
36. Fujitani M, Matsumura S, Masuda D, Yamashita S, Fushiki T, Inoue K (2014) CD36, but not GPR120, is required for efficient fatty acid utilization during endurance exercise. *Biosci Biotechnol Biochem* 78(11):1871–1878. 10.1080/09168451.2014.940835 [PubMed: 25070011]
37. Kim J, Lim K (2016) Relationship between FAT/CD36 protein in skeletal muscle and whole-body fat oxidation in endurance-trained mice. *J Exerc Nutr Biochem* 20(4):48–52. 10.20463/jenb.2016.0057
38. Manio MCC, Matsumura S, Masuda D, Inoue K (2017) CD36 is essential for endurance improvement, changes in whole-body metabolism, and efficient PPAR-related transcriptional responses in the muscle with exercise training. *Physiol Rep* 5(10):e13282. 10.14814/phy2.13282 [PubMed: 28526781]
39. Yanai H, Watanabe I, Ishii K et al. (2007) Attenuated aerobic exercise capacity in CD36 deficiency. *J Med Genet* 44(7):445–447. 10.1136/jmg.2007.050070 [PubMed: 17412877]
40. McFarlan JT, Yoshida Y, Jain SS et al. (2012) In vivo, fatty acid translocase (CD36) critically regulates skeletal muscle fuel selection, exercise performance, and training-induced adaptation of fatty acid oxidation. *J Biol Chem* 287:23502–23516. 10.1074/jbc.M111.315358

Research in context

What is already known about this subject?

- Athletes exhibit increased muscle insulin sensitivity, despite increased intramuscular triacylglycerol (TAG) content, which has been implicated in the pathogenesis of type 2 diabetes
- Recent findings suggest that the subcellular distribution of *sn*-1,2-diacylglycerols (DAGs) in the plasma membrane is a crucial pathway to induce insulin resistance

What is the key question?

- Does aerobic exercise preserve muscle insulin sensitivity, despite increasing intramuscular TAG content, by preventing increases in plasma membrane *sn*-1,2-DAGs and activation of novel PKCs (PKC ϵ and PKC θ)?

What are the new findings?

- Despite similar muscle TAG content, wheel-running mice (RC-EXE) manifested preserved muscle insulin sensitivity compared with high-fat diet-fed (HFD) mice
- HFD mice manifested increased plasma membrane *sn*-1,2-DAG content compared with the regular chow-fed (RC) mice and RC-EXE mice, which was associated with an increase in PKC ϵ and PKC θ translocation
- HFD mice also manifested an increase in IRK^{T1150} phosphorylation (a target of PKC ϵ) and decreased insulin-stimulated IRS-1-associated PI3-kinase activity (a target of PKC θ) and IRK^{Y1162} phosphorylation, compared with RC and RC-EXE mice

How might this impact on clinical practice in the foreseeable future?

- These results provide additional support for the hypothesis that the plasma membrane *sn*-1,2-DAG→PKC ϵ /PKC θ pathway causes lipid-induced muscle insulin resistance, which in turn represents a potential therapeutic target to treat muscle insulin resistance

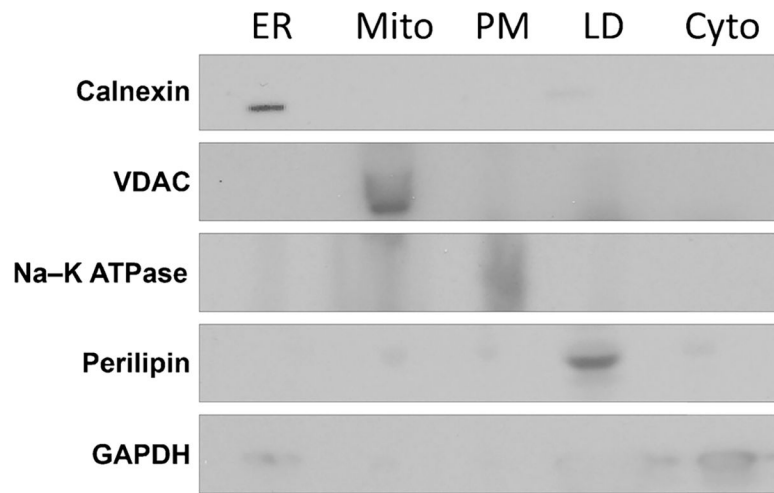


Fig. 1. Separation of five subcellular compartments in gastrocnemius measured by western blot. Cyto, cytosol; VDAC, voltage-dependent anion channel

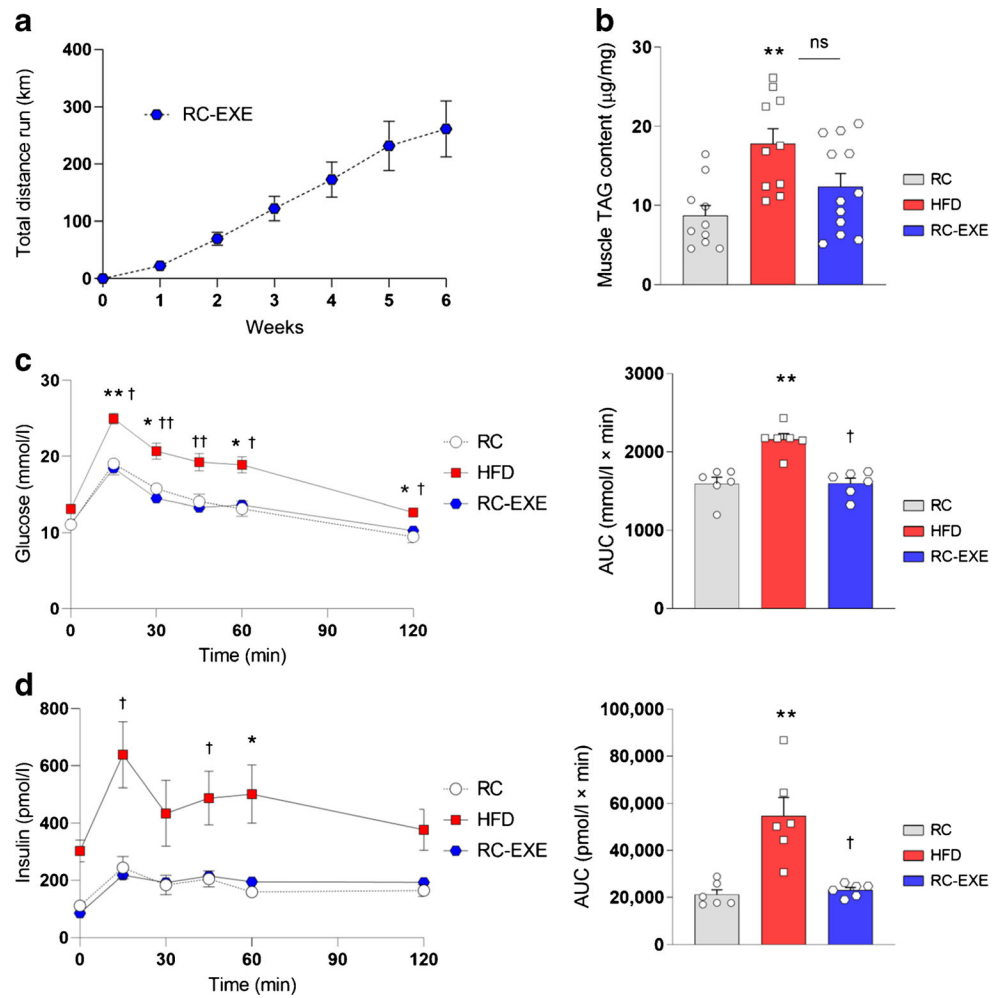
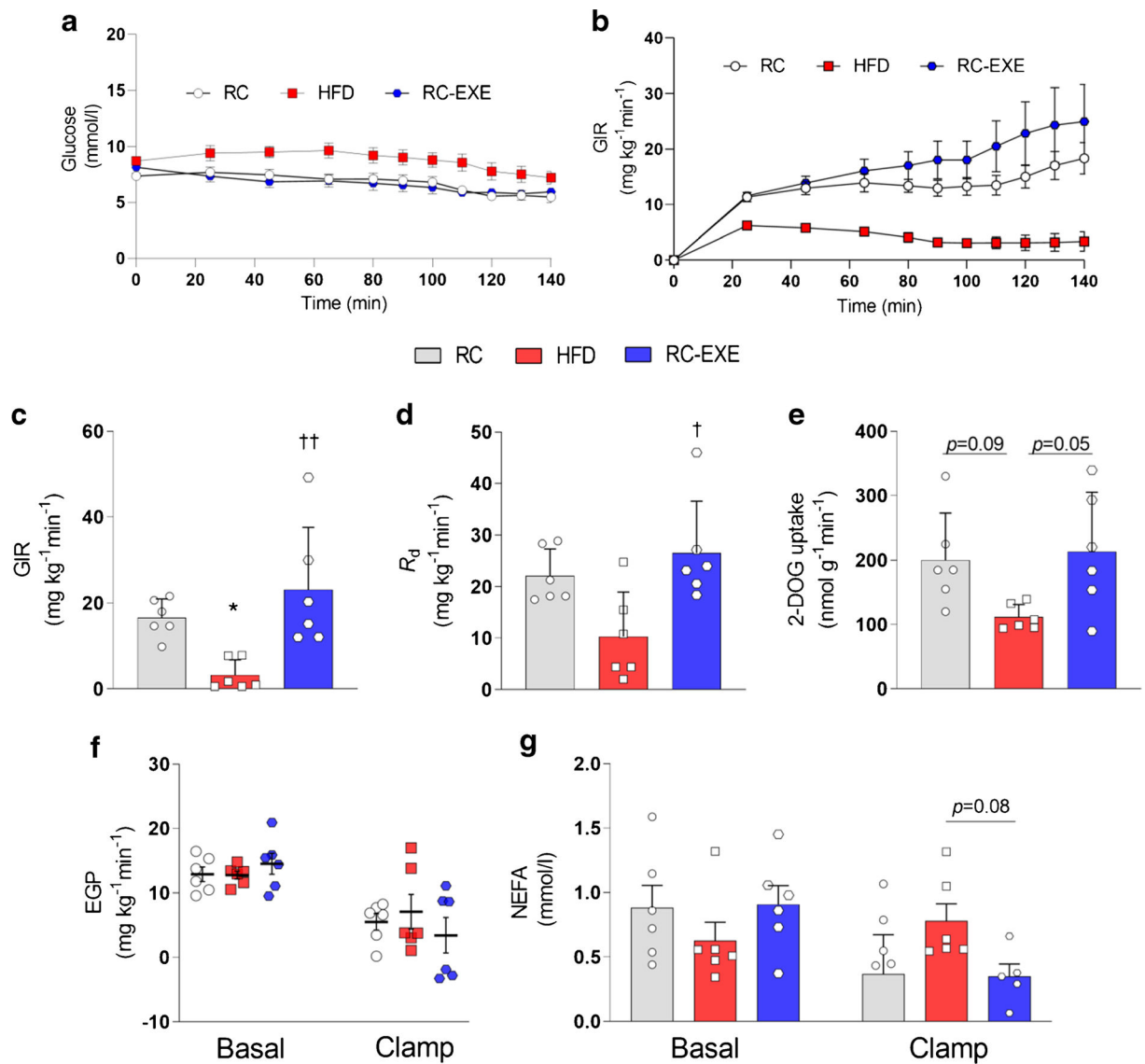


Fig. 2. Exercised mice have normal glucose tolerance despite similar muscle TAG content to HFD mice. Data are mean \pm SEM. **(a)** Distance evolution on running wheels over 6 weeks. **(b)** Gastrocnemius TAG content. **(c)** Plasma glucose levels and OGTT glucose AUC. **(d)** Plasma insulin levels and OGTT insulin AUC. After data normality analysis ANOVA was used to identify the statistical differences. * $p < 0.05$ and ** $p < 0.01$ vs RC mice; † $p < 0.05$ and †† $p < 0.01$ vs HFD mice. In **(a)**, $n = 7$ mice. In **(b)**, $n = 10$ –12 per group. In **(c)** and **(d)**, $n = 6$ per group

**Fig. 3.**

Exercised mice manifest normal insulin sensitivity in muscle despite no significant differences in muscle TAG content compared with HFD mice. Data are mean \pm SEM, $n=6$ mice per group. (a) Plasma glucose. (b) GIR. (c) Mean GIR during the hyperinsulinaemic–euglycaemic clamp. (d) Mean glucose R_d . (e) Gastrocnemius 2-DOG uptake. (f) EGP. (g) Plasma NEFA concentrations during basal and clamp periods. After data normality analysis ANOVA was used to identify the statistical differences. * $p<0.05$ vs RC mice; † $p<0.05$ and †† $p<0.01$ vs HFD mice

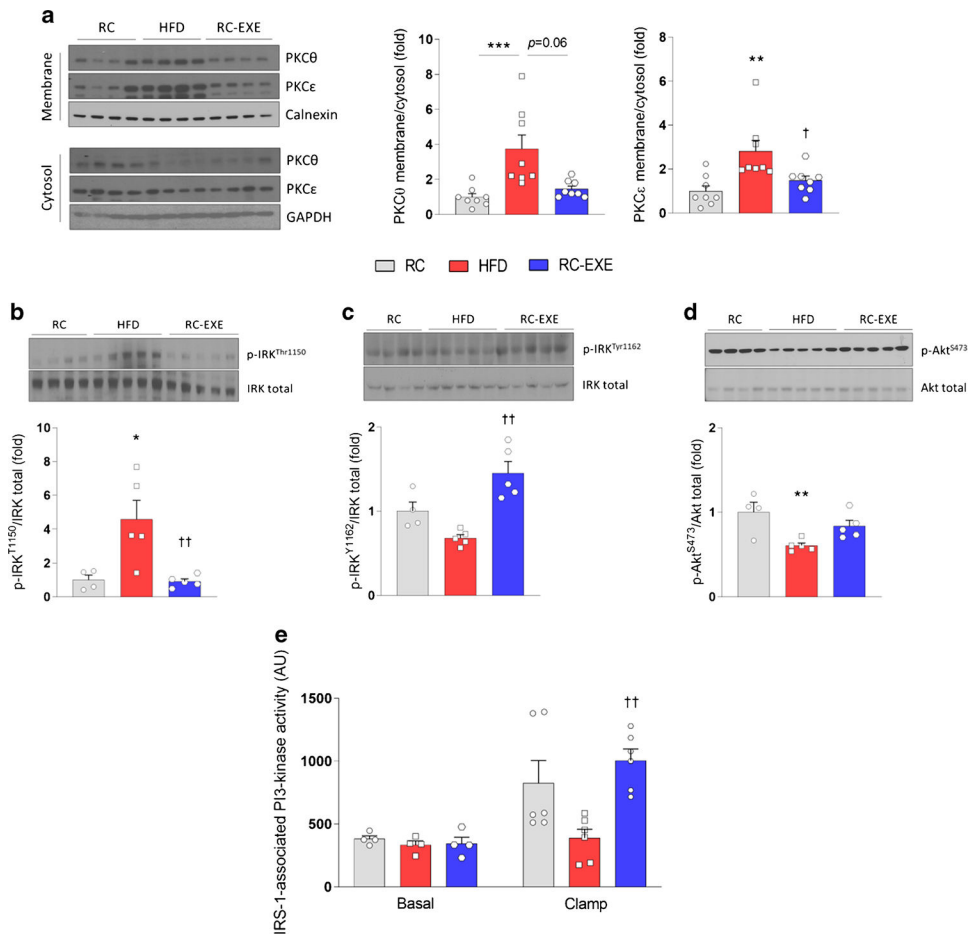


Fig. 4. Exercised mice have lower PKCε/PKCθ activation and IRK^{T1150} phosphorylation in skeletal muscle compared with HFD mice. Data are mean ± SEM. (a) PKCθ and PKCε translocation (membrane/cytosol). (b) IRK^{T1150}/IRK total. (c) IRK^{Y1162}/IRK total. (d) Akt^{S473}/Akt total. (e) IRS-1-associated PI3-kinase activity. After data normality analysis ANOVA was used to identify the statistical differences. * $p < 0.05$, ** $p < 0.01$ and *** $p < 0.001$ vs RC mice; † $p < 0.05$ and †† $p < 0.01$ vs HFD mice. In (a) and (b), $n = 8$. In (c–e), RC $n = 4$, HFD $n = 5$ and RC-EXE $n = 5$ mice. In (f), $n = 4$ basal and $n = 6$ clamp. AU, arbitrary units

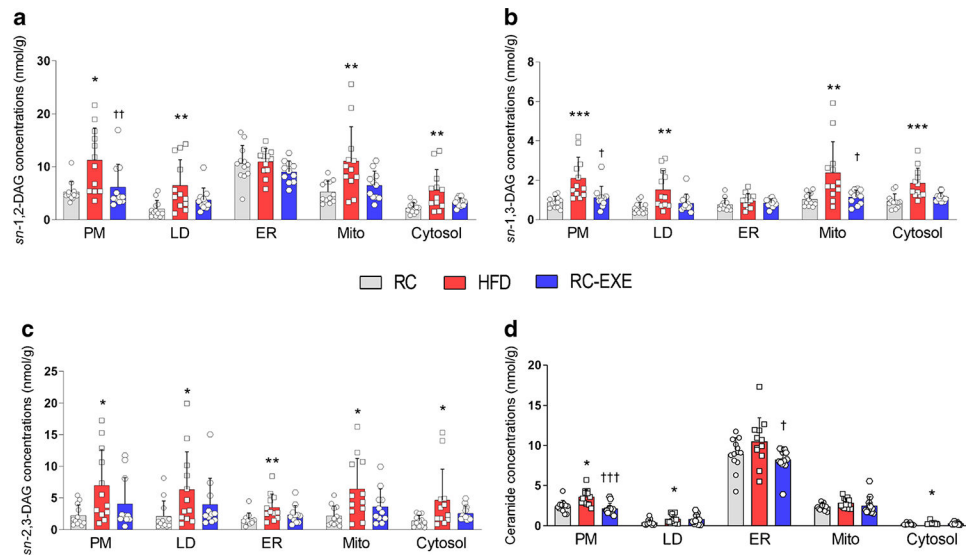


Fig. 5. *sn*-DAG and ceramide compartmentation is different in exercised mice compared with HFD mice. Data are mean \pm SEM, $n=11-12$ mice per group. **(a)** Gastrocnemius *sn*-1,2-DAG. **(b)** Gastrocnemius *sn*-1,3-DAG. **(c)** Gastrocnemius *sn*-2,3-DAG. **(d)** Gastrocnemius ceramide concentrations. After data normality analysis ANOVA was used to identify the statistical differences. * $p<0.05$, ** $p<0.01$ and *** $p<0.001$ vs RC mice; † $p<0.05$, †† $p<0.01$ and ††† $p<0.001$ vs HFD mice

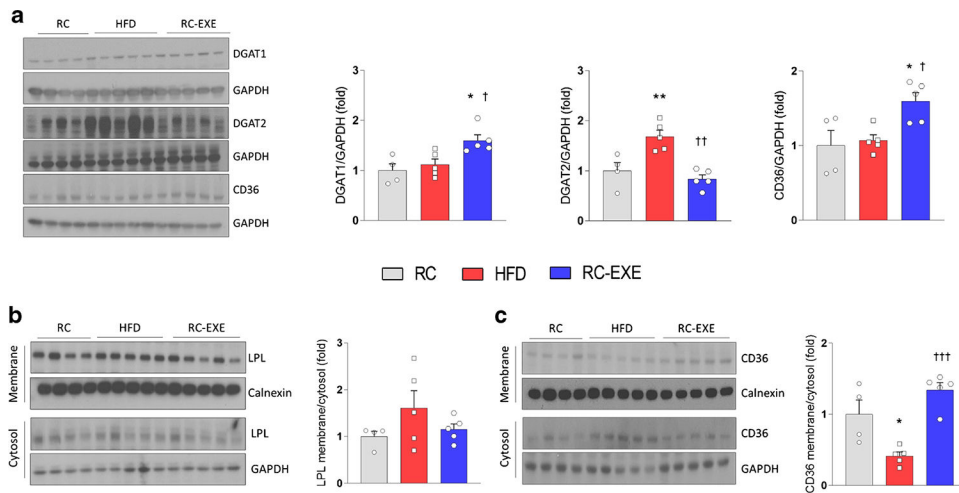


Fig. 6. Exercised mice had increased DGAT1 and CD36 in skeletal muscle. Data are mean \pm SEM (RC $n=4$, HFD $n=5$ and RC-EXE $n=5$ mice). **(a)** DGAT1/GAPDH, DGAT2/GAPDH and CD36/GAPDH. **(b)** LPL translocation (membrane/cytosol). **(c)** CD36 translocation (membrane/cytosol). After data normality analysis ANOVA was used to identify the statistical differences. * $p<0.05$ and ** $p<0.01$ vs RC mice; † $p<0.05$, †† $p<0.01$ and ††† $p<0.001$ vs HFD mice

Table 1

Baseline characteristics of mice

Characteristic	RC	HFD	RC-EXE
Initial BW (g)	27.6 ± 2	26.9 ± 1.7	27.8 ± 0.8
Final BW (g)	28.8 ± 1.2	33.3 ± 2.5 ^{***}	27.8 ± 1.1 ^{†††}
Fat mass (%)	2.3 ± 0.9	10.2 ± 5.4 ^{***}	2.9 ± 0.6 [†]
Lean mass (%)	76.3 ± 2.4	66.7 ± 5.9 ^{***}	73.3 ± 2.8 [†]
Muscle glycogen (μmol/g)	18.5 ± 4.6	17.7 ± 5.7	19.7 ± 3.1

Data are mean ± SEM

n=6–8 mice per group

^{***}
p<0.001 vs RC mice

[†]
p<0.05 and

^{†††}
p<0.001 vs HFD mice

BW, body weight

Author Manuscript

Author Manuscript

Author Manuscript

Author Manuscript